High-resolution LES of the rotating stall in a reduced scale model pump-turbine

Olivier Pacot[1], **Chisachi Kato**[2] **and François Avellan**[1]

[1] EPFL Laboratory for Hydraulic Machines, Av. de Cour 33bis, 1007 Lausanne, Switzerland.
[2] Institute of Industrial Science, The University of Tokyo, 4-6-1 Komaba, Meguro-ku, Tokyo 153-8505, Japan

E-mail: olivier.pacot@epfl.ch

Abstract. Extending the operating range of modern pump-turbines becomes increasingly important in the course of the integration of renewable energy sources in the existing power grid. However, at partial load condition in pumping mode, the occurrence of rotating stall is critical to the operational safety of the machine and on the grid stability. The understanding of the mechanisms behind this flow phenomenon yet remains vague and incomplete. Past numerical simulations using a RANS approach often led to inconclusive results concerning the physical background. For the first time, the rotating stall is investigated by performing a large scale LES calculation on the HYDRODYNA pump-turbine scale model featuring approximately 100 million elements. The computations were performed on the PRIMEHPC FX10 of the University of Tokyo using the overset Finite Element open source code FrontFlow/blue with the dynamic Smagorinsky turbulence model and the no-slip wall condition. The internal flow computed is the one when operating the pump-turbine at 76% of the best efficiency point in pumping mode, as previous experimental research showed the presence of four rotating cells. The rotating stall phenomenon is accurately reproduced for a reduced Reynolds number using the LES approach with acceptable computing resources. The results show an excellent agreement with available experimental data from the reduced scale model testing at the EPFL Laboratory for Hydraulic Machines. The number of stall cells as well as the propagation speed corroborates the experiment.

1. Introduction

The constant increase of the energy demand and the will to decrease the use of ressources generating greenhouse gas push countries and electricity industries to develop the renewable energies, as for example the wind energy, the solar energy and the hydraulic energy. These energies have the advantage to have a low impact on the environment, but are weather dependent and, therefore, provide an amount of energy which highly fluctuates. To integrate them on the existing power grid, it is required to develop a technology able to respond to any change of the supply and the demand, hence to guarantee a stable power grid. A technology with such a capability is the pumped-storage power plant, because it can almost instantaneously produce electricity when the demand is high and store the energy when the supply becomes higher than the demand. However, for economical reasons, the initial pump and water turbine were merged into a single machine, called pump-turbine, which should have the capacity to work in a large operating range. Such a requirement is difficult to meet as instabilities arise when the machine is operated at off-design conditions. One example is the appearance of the rotating stall when a

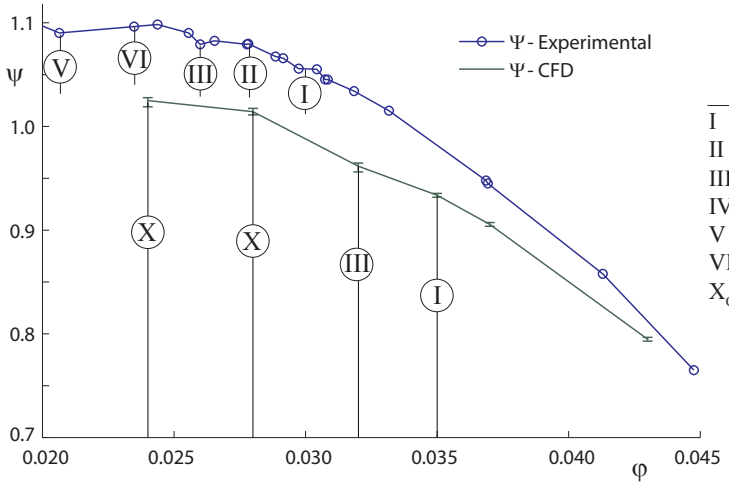

	φ_{EXP}	φ_{CFD}	$k_{s\text{-}EXP}$	$\omega_{s\text{-}EXP}$	$\omega_{s\text{-}CFD}$
I	0.030	0.034	incipient stall		
II	0.028	-	3	0.016 ω	–
III	0.026	0.032	4	0.021 ω	0.029 ω
IV	0.024	-	5	0.024 ω	–
V	0.021	-	5	0.014 ω	–
VI	0.015	-	4	0.028 ω	–
X_{CFD}	-	<0.030	Evenly distributed stall		

Figure 1. Comparison of experimental and numerical results, energy coefficient and stall modes. Data obtained from [7].

pump-turbine is operated at part load condition. Such an instability induces a loss of efficiency, vibration and even cavitation which can seriously damage the machine. Hence the high need to predict such a phenomenon.

Up to this day, only a few experimental studies [1–3] and numerical studies [4–6] were dedicated to the rotating stall phenomenon in a vaned diffuser. Experimentally, the main issue is the difficulty to get an optical access in the machine to visualize the flow and numerically, the difficulty is to reproduce accurately the phenomenon. In the study of Braun [7], both experimental and numerical investigations of the rotating stall in the diffuser of a pump-turbine were performed. It was shown that the standard RANS approach using the k-ω SST model failed to reproduce accurately the phenomenon. Indeed, the flow rate had to be increased by 23% in order to observe the presence of the stall cells and the corresponding computed propagation speed was 38% faster compared to the experiment, see figure 1.

Thanks to the constant development of the computing power since the 70s, the size of the actual supercomputers offers new opportunities in numerical simulation. For instance, the well known Large Eddy Simulation (LES) approach was so far not used as this approach is time consuming and requires large computing ressources. The reason is specific to the approach as all the main structures in the flow have to be captured in order to obtain an accurate solution. Therefore, a sufficiently fine mesh has to be generated, which in almost all industrial-type investigations is not feasible, because of the size of the required mesh. However, a feasibility study showed that for a reduced Reynolds number and using an actual supercomputer, the investigation of rotating stall in a pump-turbine at 76% of the best efficiency point in pumping mode is practicable [8]. For a Reynolds number reduced by 25 compared to the experiment, the required mesh size is 80 millions elements and 2,048 cores are sufficient to compute the unsteady flow field.

The present work describes the numerical setup to compute the rotating stall phenomenon by LES and provides the results for a selected operating point.

2. Numerical Setup

2.1. Governing Equations

The governing equations to compute incompressible flows by the LES method are the low-pass filtered continuity equation and the incompressible low-pass filtered Navier-Stokes equations:

$$\frac{\partial \overline{C}_i}{\partial x_i} = 0 \tag{1}$$

$$\frac{\partial \overline{C}_i}{\partial t} + \overline{C}_j \frac{\partial \overline{C}_i}{\partial x_j} = -\frac{1}{\rho}\frac{\partial \overline{p}}{\partial x_i} + \frac{\partial}{\partial x_j}\left[\nu\left(\frac{\partial \overline{C}_i}{\partial x_j} + \frac{\partial \overline{C}_j}{\partial x_i}\right) - \tau_{ij}\right] \tag{2}$$

where $\overline{C}_i$ is the filtered velocity component, $\overline{p}$ is the filtered static pressure, ρ is the fluid density, ν is the fluid kinematic viscosity and τ_{ij} is the subgrid scale tensor (SGS), defined as:

$$\tau_{ij} = \overline{C_i C_j} - \overline{C}_i \overline{C}_j \tag{3}$$

To close the system of equations, the Smagorinsky model defined as follow is used:

$$\tau_{ij} - \frac{1}{3}\delta_{ij}\tau_{ij} = -2\nu_{sgs}\overline{S}_{ij} \tag{4}$$

with

$$\nu_{sgs} = (C_s\Delta)^2\sqrt{2\overline{S}_{ij}\overline{S}_{ij}} \tag{5}$$

and

$$\overline{S}_{ij} = \frac{1}{2}\left(\frac{\partial \overline{C}_i}{\partial x_j} + \frac{\partial \overline{C}_j}{\partial x_i}\right) \tag{6}$$

2.2. Numerical Method

The filtered incompressible Navier-Stokes equations are solved using the Fractional Step (FS) method with the Crank-Nicolson (CN) implicit time integration scheme. The spatial discretization is performed by the Galerkin Finite Element Method. The resulting linear systems of equations are solved by the Bi-CGSTAB wrapped with the residual cutting method (RCM). The numerical code has a multiple frame of references implemented and uses an overset grid as interface.

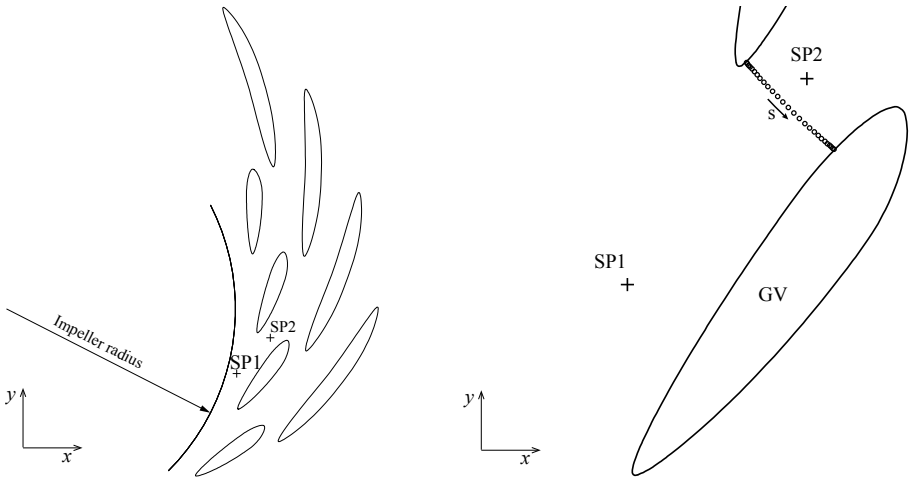

Figure 2. Left: Location of the pressure sampling points (SP1 and SP2). Right: Zoom on the guide vane passage and location of the sampling surface for the flow rate monitoring, shown by the circles.

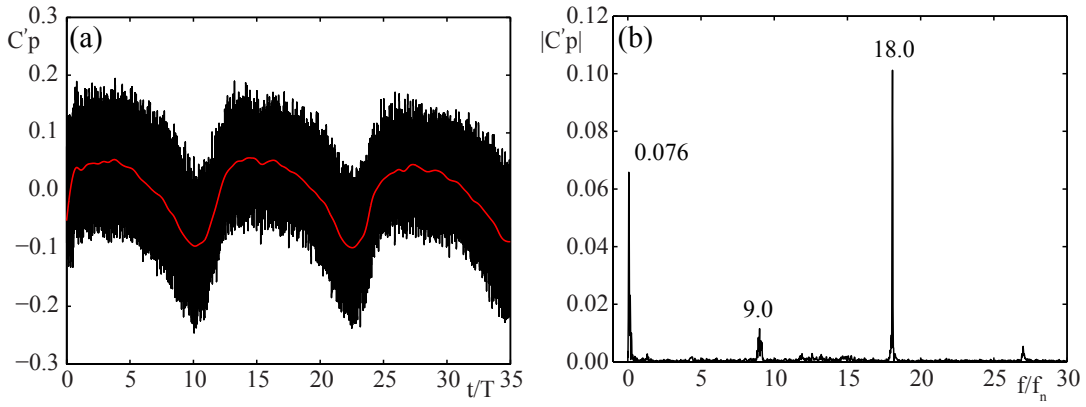

Figure 3. (a) Time history of the pressure coefficient fluctuation at SP1. The red curve is the pressure coefficient fluctuation that is low-pass filtered using a cutoff frequency equal to f_n. (b) Discrete Fourier Transform of the instantaneous pressure coefficient fluctuation.

2.3. Computation Setup

The mesh used to compute the flow is composed of 85 millions hexahedral elements and the computations were performed using 2,048 cores on the supercomputer PRIMEHPC FX10, which belongs to the University of Tokyo. FX10 is equipped with the new CPU generation of SPARC64 IXfx, which is composed of 16 cores running at 1.848 GHz with 12MB of L2 cache. The pump-turbine is operating in pumping mode and at a part load condition, Q/Q_{BEP}=76%, with the corresponding part load flow coefficient φ=0.026; BEP standing for best efficiency point.

3. Rotating Stall

3.1. Propagation Speed

The presence of the rotating stall phenomenon in the diffuser affects both the velocity field and the pressure field. To monitor its presence, one can set pressure sampling points in each diffuser passage, as shown in figure 2. Figure 3 (a) shows the time history of the pressure coefficient fluctuation at SP1 during 35 impeller revolutions. The red curve is the pressure coefficient fluctuation that is low-pass filtered using a cutoff frequency equal to f_n. A clear fluctuation with a low frequency is observable, which is confirmed by the Discrete Fourier Transform of the instantaneous pressure coefficient fluctuation, see figure 3 (b). Indeed, three different peaks are present, where the ones at 9 and 18 represent the blade passing frequency and its first harmonic, respectively. The first peak is the result of the low propagation of the stall cells. Experimentally, 4 stall cells propagating at $\omega_s/\omega = 2\%$ are reported to take place for this operating condition [7]. Therefore, each sampling point will see four times this speed. The peak at f/f_n=7.6% confirms the presence of four stall cells. However, this approach is not suitable to provide an accurate propagation speed, as it requires a too long time history to get an acceptable normalized frequency resolution. To overcome this issue, the flow rate passing through each guide vane passage is monitored at each time step and for each guide vane channel, that is 20 passages. The location of the sampling surface is shown in the right side of figure 2 with black circles.

Figure 4 shows the instantaneous flow rate through 4 guide vane channels, each separated by 5 channels, as the pattern of one stall cell occupies 5 guide vane channels. As it can be seen, the rates of flow rate increase and decrease are almost constant. Furthermore, the data is averaged with respect to the stall phase and the result is shown by the black curve in figure 4. The stall phase is obtained by calculating an analytic signal of the pressure located at SP1 during 35

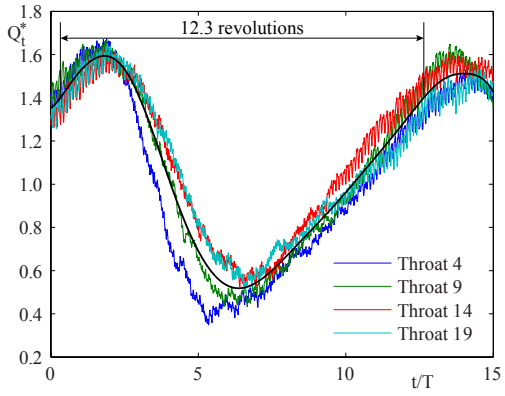

Figure 4. Instantaneous flow rate through 4 guide vane channels each separated by 5 channels. The black curve is the resulting phase average.

impeller revolutions, according to:

$$\mathcal{P}(t) = \tilde{p'}(t) + i\mathcal{H}(\tilde{p'}(t)) \tag{7}$$

where $\tilde{p'}$ is the fluctuation of the low-pass filtered pressure and $\mathcal{H}(\tilde{p'})$ its Hilbert transform. The analytic amplitude and analytic phase are respectively $a(t) = |\mathcal{P}(t)|$ and $\phi(t) = arg|\mathcal{P}(t)|$. This decomposition is reversible and the original signal can be reconstructed using:

$$\tilde{p'}(t) = a(t)cos(\phi(t)) \tag{8}$$

Figures 5 a) and b) show respectively the analytic phase and the analytic amplitude of the pressure signal at SP1 shown in figure 3 (a). The three cycles displayed in figure 3 (b) correspond to three passages of a stall cell. The analytic phase ϕ is, henceforth, referred to as stall phase.

Such an average has been used to estimate the number of impeller revolutions required to reach back to the initial condition for the individual channel. It takes 12.3 impeller revolutions for a channel to see the full passage of one stall cell. Using this evaluation, 49.3 impeller revolutions are required for one full stall cycle, which results in a normalized propagation speed of $\omega_s/\omega = 2.03\%$. This result is very satisfactory as it is only 3.4% slower than that of the measurement.

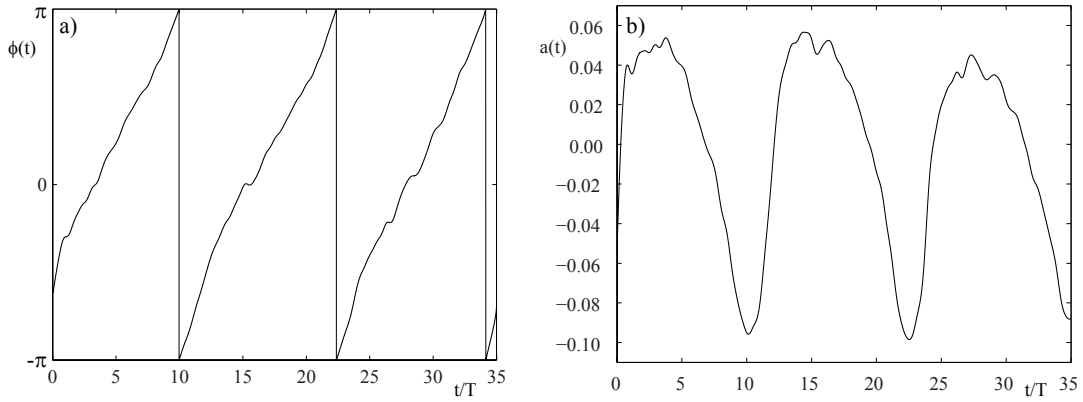

Figure 5. Analytic signal of the low-pass filtered pressure fluctuation signal shown in figure. 3 (a): a) analytic/stall phase, b) analytic amplitude.

3.2. Propagation Mechanism

The propagation mechanism of the rotating stall may be regarded as the local growth and decay of a stall cell and the rate of fluctuation of a stall cell governs the propagation speed. To illustrate this behavior, the flow patterns in a guide vane channel are schematically represented in figure 6 for 6 specific instants. During the phase where the flow rate is increasing, figures 6 a) and b), no recirculation is observable, but the adverse pressure between SP1 and SP2 is increasing as well as the Angle Of Attack (AOA) of the flow on the upstream guide vane. Such increases lead to favorable conditions for flow separation and the appearance of the stall cell. The growth of this stall cell reduces firstly the flow rate passing through the guide vane channel in figure 6c), and almost blocks the channel when the stall cell reaches its maximum size in figure 6d), i.e. when it reaches the leading edge of the downstream guide vane. Since, on the one hand the flow velocity at the inlet of the guide vane is decreasing and, consequently, the adverse pressure is decreasing and on the other hand the AOA of the flow on the upstream guide vane is decreasing, the conditions are unfavorable for the stall cell to sustain in figure 6e). This results in a decay of the stall cell and accordingly an increase of the flow rate.

The growth and decay are governed by the variation of the adverse pressure gradient between the leading and the trailing edges of the guide vane and by the deviation of the flow near the leading edge of a guide vane. Furthermore, as the recirculation is located in a narrowed area, it induces a modification of the flow as soon as the recirculation zone grows. Therefore, any changes in the size of the recirculation zone change the flow pattern near the leading edge of the downstream guide vane. These changes are responsible for the switch between the favorable and the unfavorable conditions for a recirculation zone to grow.

4. Conclusion

A large scale computation of the rotating stall phenomenon was performed for the first time using the Large Eddy Simulation technique. The case study selected is the reduced scale model pump-turbine HYDRODYNA, operating at part load condition (76% BEP) in pumping mode. The computations were performed using the open source software FrontFlow/Blue and the PRIMEHPC FX10 supercomputer of the University of Tokyo.

The simulation for a reduced Reynolds number (Re/25) with regards to the experiment produced an accurate and satisfactory outcome. The number of stall cells was correctly captured and the propagation speed was only 3.4% slower than the measured value. Furthermore, the computed specific energy coefficient Ψ showed an excellent agreement with the experiment as it is only 0.36% higher compared to the measurement. It is concluded that the LES approach is a powerful tool, whereas the traditional RANS approach rapidly reaches its limits.

This analysis showed that the stall mechanism is driven by the growth and the decay of the stall cell. Furthermore, it was shown that both the rate of growth and the rate of decay are almost constant, where the rate of growth is higher than the rate of decay. The stall cell is located at the guide vane trailing edge on the suction side. As soon as it starts growing, the flow within the guide vane channel is deviated towards the downstream channel. The growth of the stall cell is such that at its maximum volume, the stall size occupies the entire guide vane pitch. However, the orientation of the flow at the guide vane inlet and the decrease of the adverse pressure gradient result in the impossibility for such a cell to sustain. The cell size decreases until the favorable conditions for flow recirculation are met again.

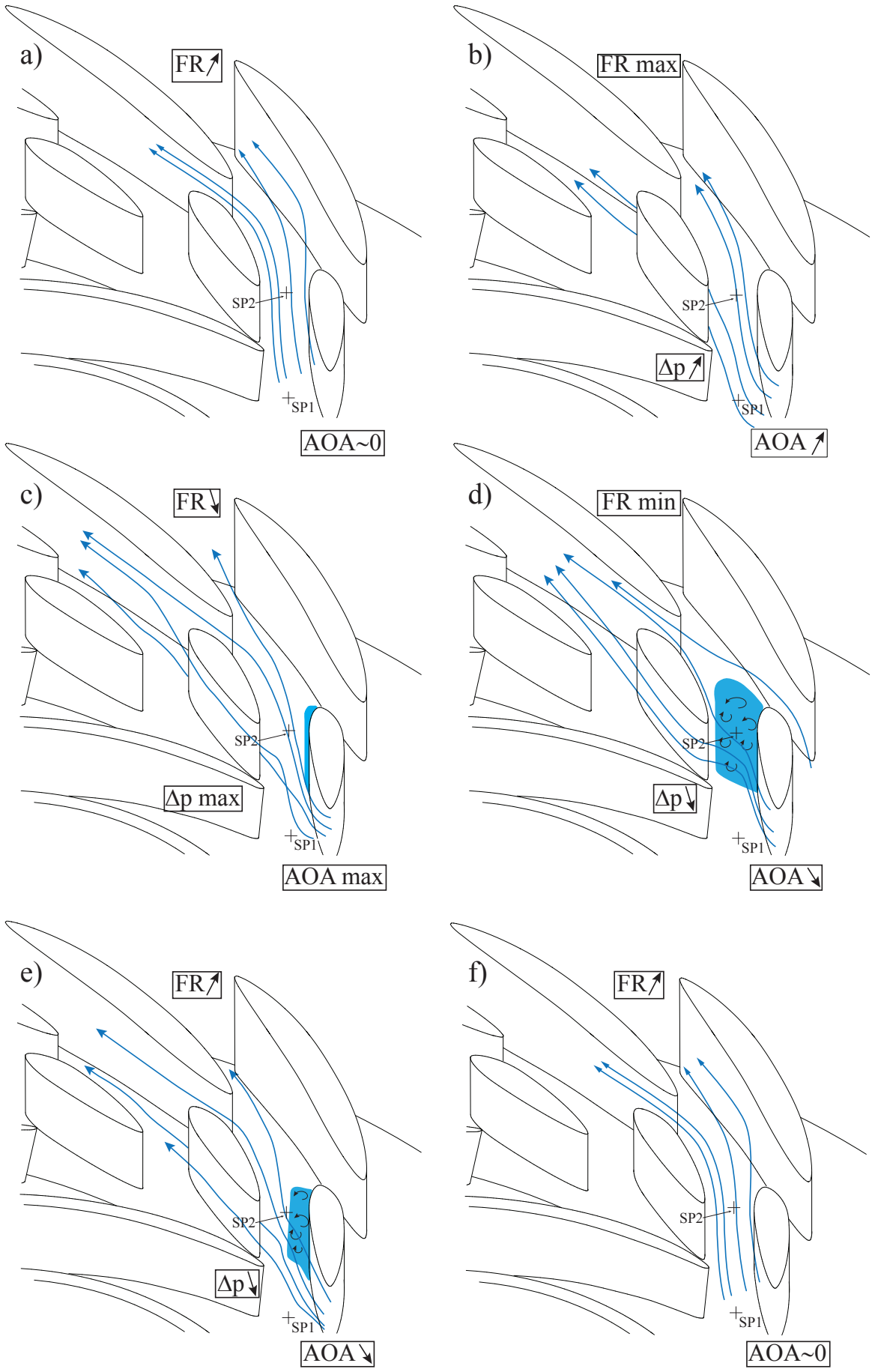

Figure 6. Schematic of the variation of the flow within a guide vane channel.

Acknowledgments
The authors would like to thank Dr. Y. Guo and Mr. Y. Yamade for all their scientific advices and for providing the numerical code. The authors would also like to thank the University of Tokyo to make the supercomputer PRIMEHPC FX10 available for this study. This research was supported by the Swiss National Science Foundation (SNSF) Grant No. 200021-130605.

References
[1] Berten S 2010 *Hydrodynamics of High Specific Power Pumps for Off-Design Operating Conditions* Ph.D. thesis EPFL
[2] Sano T, Nakamura Y, Yoshida Y and Tsujimoto Y 2002 *JSME International Journal Series B* **45** 810–819
[3] Sinha M, Pinarbasi A and Katz J 2001 *Journal of Fluids Engineering* **123** 490–499
[4] Byskov R K, Jacobsen C B and Pedersen N 2003 *Journal of Fluids Engineering* **125** 73–83
[5] Lucius A and Brenner G 2010 *International Journal of Heat and Fluid Flow* **31** 1113–1118
[6] Sano T, Yoshida Y, Tsujimoto Y, Nakamura Y and Matsushima T 2002 *Journal of Fluids Engineering* **124** 363–370
[7] Braun O 2009 *Part Load Flow in Radial Centrifugal Pumps* Ph.D. thesis EPFL
[8] Pacot O 2014 *Large Scale Computation of the Rotating Stall in a Pump-Turbine using an Overset Finite Element Large Eddy Simulation Numerical Code* Ph.D. thesis EPFL